Fermilab

Fermi National Accelerator Laboratory
P.O. Box 500 • Batavia, Illinois • 60510

**TD – 01 – 036**
**May 25, 2001**

# $Nb_3Sn$ Cos($\theta$) Dipole Magnet, HFDA-02 Production Report

**D. R. Chichili[1], N. Andreev[1], E. Barzi[2], V.V. Kashikhin[2], I. Terechkine[1], S. Yadav[1], R. Yamada[2], and A.V. Zlobin[2]**

*[1]Engineering and Fabrication Department*
*[2]Development and Test Department*
*Technical Division*
*Fermilab, Batavia, IL 60510*

# 1.0 INTRODUCTION

HFDA-02 is the second $Nb_3Sn$ shell-type magnet to be fabricated and the first to be tested. The dipole model is a 1 m long magnet with 43.5 mm bore aperture. Fig. 1 shows the completed magnet ready to be tested. The magnet design is identical to HFDA-01[*]. The fabrication procedure followed is also similar to HFDA-01 with some modifications to address the problems encountered during the first magnet production.

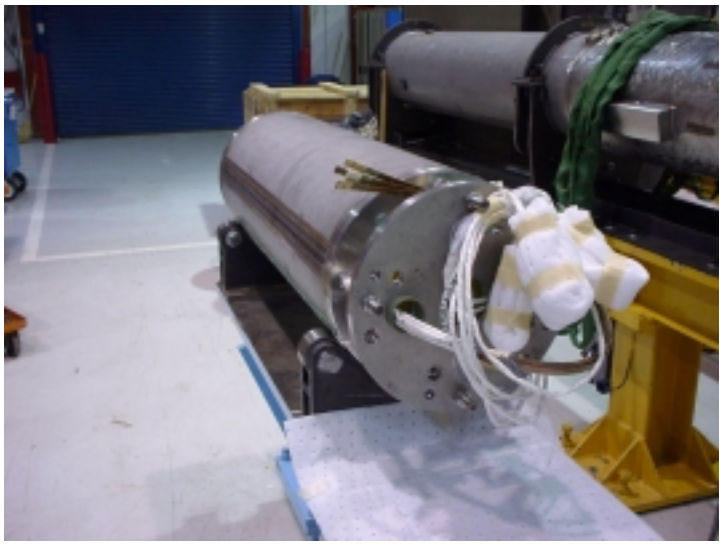

**Fig. 1**: *Photograph of HFDA-02*.

The specific features of HFDA-02 are listed below:

- The coil size after curing was optimized such that after reaction the coils will be at the nominal size. This precaution was taken to eliminate excessive pressure on the conductor during reaction. See Section-3 for details.

- The reaction cycle was modified to have a low temperature step in the beginning to allow tin to diffuse in solid phase. This low temperature step was added to avoid tin-leakage. See Section-4 for details.

- The coil end-parts were optimized for better conductor support. Further the end-parts were manufactured using water-jet machining which is more cost effective compared to conventional 5-axis CNC machining. See Section-3 for details.

- Ground Insulation was modified from three layers of 0.125 mm thick ceramic cloth to two layers of 0.25 mm thick ceramic cloth.

- Quench protection heaters were installed between the two layers of ground insulation. In HFDA-01, there were weaved on to the middle layer of the three layer interlayer insulation.

[*] HFDA-01 Production Report, TD-00-069

- Unlike in HFDA-01, no voltage taps were installed in the coil during winding. They were installed only on the lead cables as per drawing MB-376907.

Most of the details of the fabrication were discussed in HFDA-01 production report. This report will summarize the fabrication steps and data collected during production of HFDA-02.

## 2.0 STRAND and CABLE

The conductor used for HFDA-02 was manufactured by OST using Modified Jelly Roll Process. The nominal diameter of the strand was 1.00 mm with an effective filament diameter of 115 μm. The Cu to non-Cu ratio was 0.92.

Rutherford type cable with 25 μm thick stainless steel core was manufactured at LBNL. The cable parameters are listed in Table 1. The first half coil, HFDAH-03 was wound with cable from Reel No. 765 and the second half coil, HFDAH-04 from Reel No. 782. The cable was initially cleaned with ABZOL-VG to remove any oil residue left from the cabling process. It was then heat-treated at 200 $^{o}$C for 30 min to reduce the residual twist in the cable that also comes from the cabling process.

| Parameter | Unit | HFDAH-03 | HFDAH-04 |
|---|---|---|---|
| Mid-Thickness | mm | 1.8204$^{\$}$ | 1.8154 |
| Width | mm | 14.234 | 14.242 |
| Keystone angle | deg | 0.92 | 0.905 |
| Pitch Length | mm | 109.8 | 109.8 |
| Number of Strands | | 28 | 28 |
| Lay Direction | | Left | Left |
| Reel Number | | 765 | 782 |

**Table 1**: *Cable parameters as provided by LBNL.* $^{\$}$*The mid-thickness of the cable was later measured at Fermilab and found to be 1.84 mm.*

The critical current for a virgin strand and an extracted strand which were placed as witness samples in the reaction fixture along with the coil was measured to be 723 A and 662 A respectively at 12 T. Based on these results, the magnet short sample limit is estimated to be 11 T at 20.08 kA.

## 3.0 COIL FABRICATION

As stated earlier, the azimuthal coil size after curing was optimized such that after reaction the coils will be at the nominal size. Further second-generation end-parts were used in HFDA-02 for better conductor support. Below is the brief description of these improvements.

## 3.1 Coil Size Optimization

Several experiments were performed to determine the correct amount of insulation overlap so that the coil will be at the nominal size after reaction. First the mean thickness of the insulation with various percentage overlaps was measured as a function of pressure. Fig. 2 shows the data. The measurements were taken using four-stack insulated cables. Second, the variation of insulation thickness during cyclic loading was measured. Fig. 3 shows the data for two cycles with 50% and 25% insulation overlap pattern. Note that there is almost 50 μm drop in thickness during the second cycle. Finally the increase in thickness of the cables due to reaction was measured. Fig. 4 shows the data for an insulated cable. Note that at a pressure of 5 MPa, the increase in thickness is about 115 μm.

With this information we decided to go with 30% overlap for HFDAH-03 and 40% overlap for HFDAH-04. The difference in the percentage overlap between the two half-coils was due to the fact that the mid-thickness of the cable from Reel No. 765 used for HFDAH-03 was found to be 1.84 mm and not 1.82 mm as reported by LBNL. So the insulation thickness had to be further reduced to take this into account. A 1 mm thick Kapton shim was placed between the azimuthal pusher bar and the coil to account for the reduction in the insulation volume.

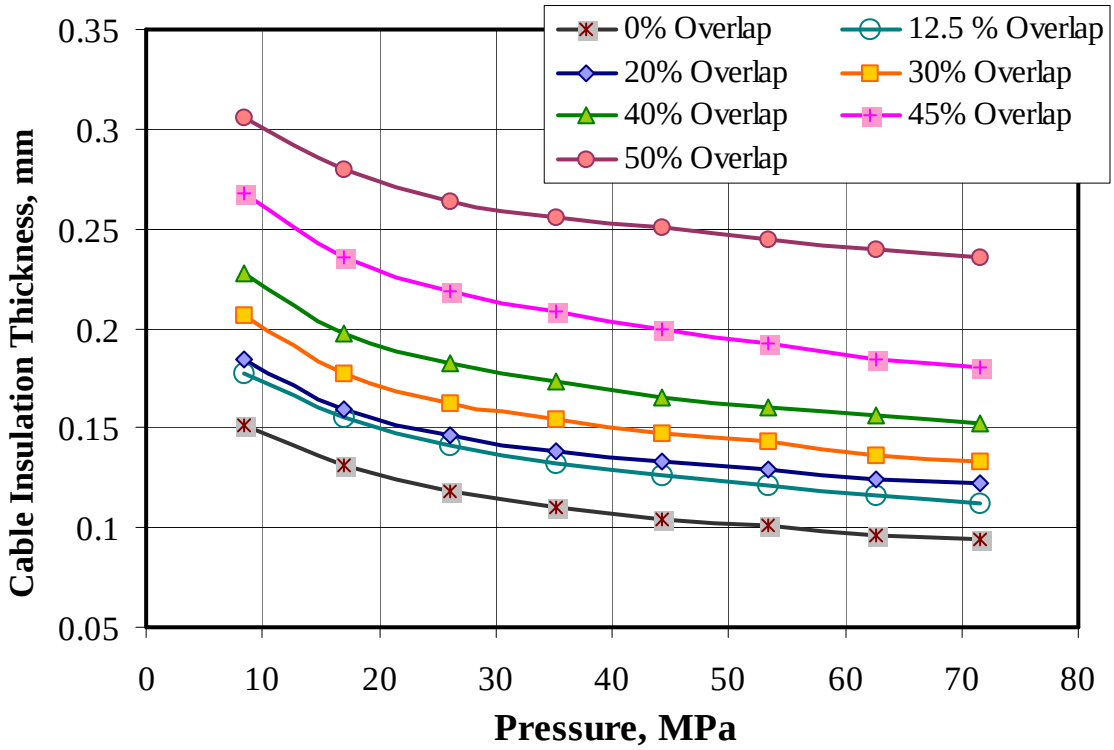


**Fig. 2**: *Variation of insulation thickness with pressure*.

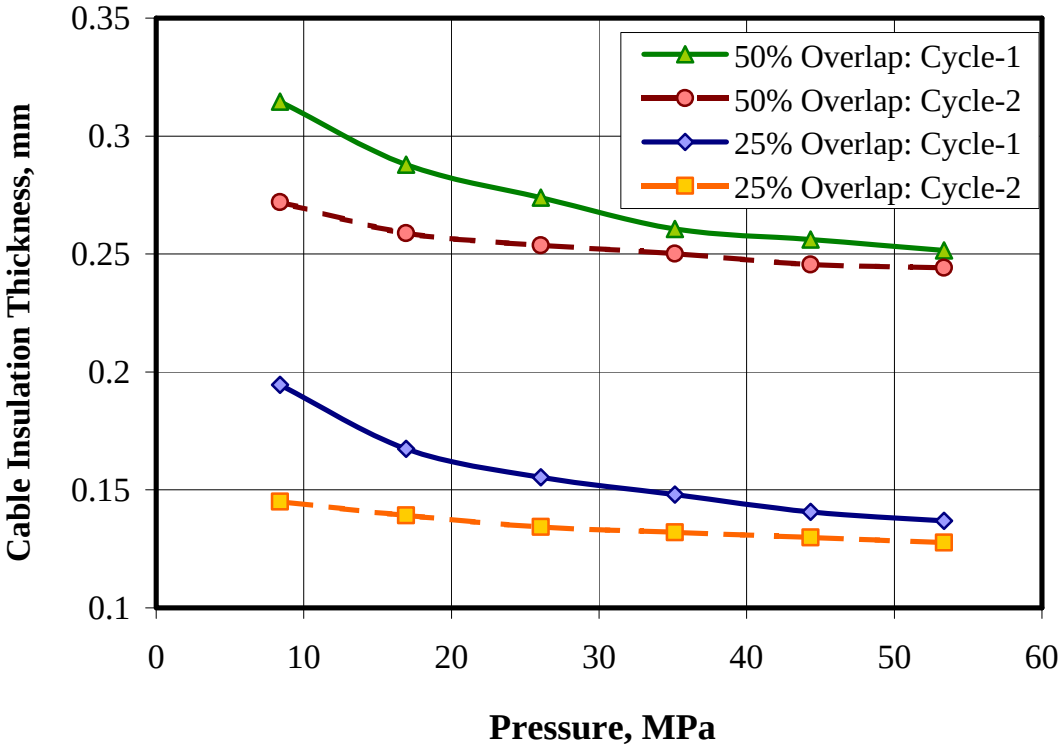


**Fig. 3**: *Variation of insulation thickness with pressure under cyclic loading*.

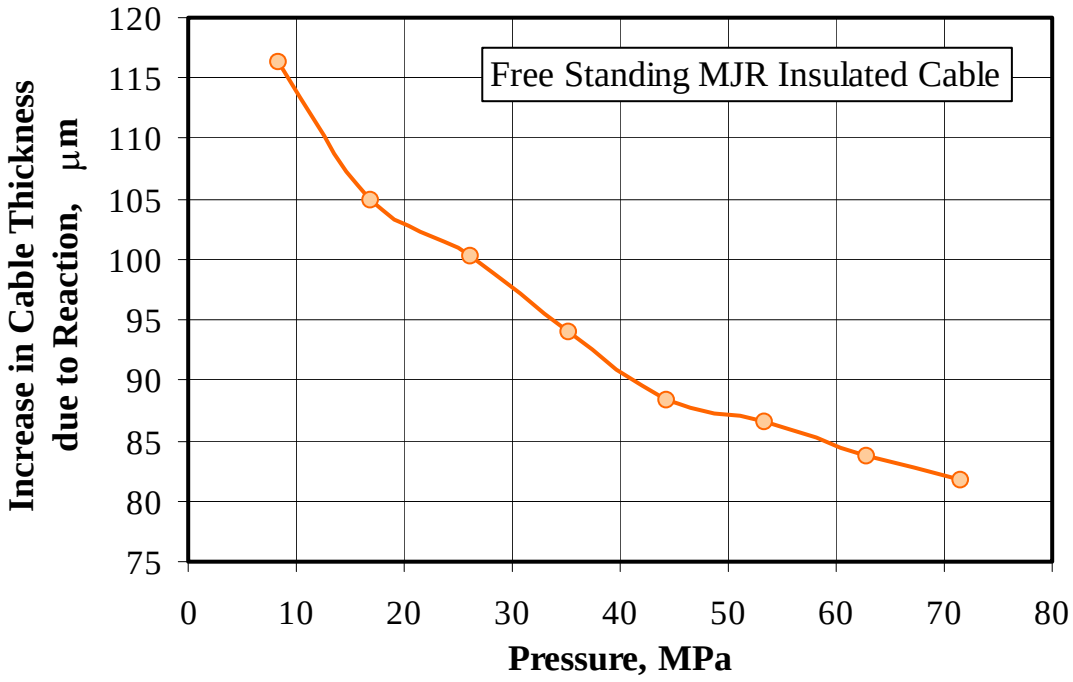


**Fig. 4**: *Cable thickness variation with pressure*.

## 3.2 Coil End-Parts

Second generation end-parts were used in HFDA-02 coils. The YZ inclination angle was optimized in this design for better conductor support. Fig. 5 shows the longitudinal section of the half-coil LE with first and second generation end-parts. The deviation from the value suggested by BEND was reduced from the first version to second version to obtain good conductor support [#].

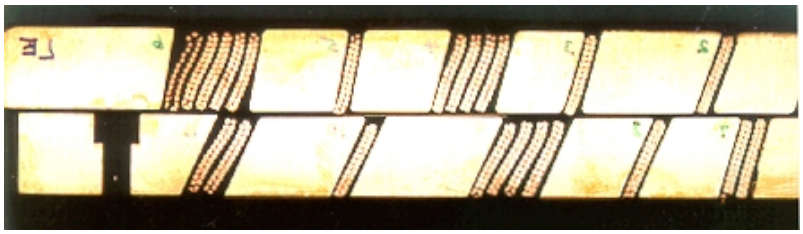

(a)

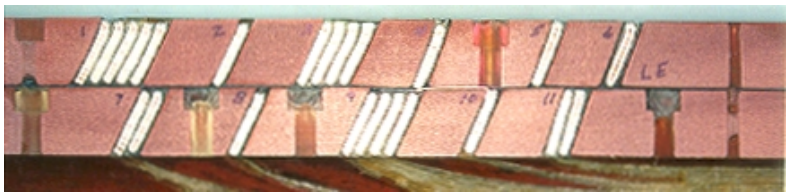


(b)

**Fig. 5:** *Longitudinal section of the half-coil LE, (a) with first generation end-parts (b) with second generation end-parts.*

The end-parts for HFDA-02 were manufactured using water-jet machining which is more cost effective than conventional 5-axis machining or EDM. However the machine shop encountered some difficulties during the fabrication due to steep angles on the 3-D surfaces of the end-parts. This resulted in some irregularities on the surface. We corrected this by applying the ceramic fiber with binder and curing it at 150 $^{o}$C for 30 min. Fig. 6 shows an end-part that has been cured with ceramic fiber and binder. Unlike in HFDA-01, the end-parts for HFDA-02 were not ceramic coated.

[#] S. Yadav, D. Chichili and I. Terechkine, "Coil Design Issues for the High Field Dipole at Fermilab", Presented at ASC-00, Vriginia Beech, September 2000.

## 3.3 Coil Winding and Curing

The two half coils were wound and cured similar to HFDA-01 coils. Fig. 7 shows the two half-coils fabricated for HFDA-02. A third curing cycle in which the ground insulation was cured on top of the half coil was added to improve the coil assembly process into the reaction fixture. Ground insulation consisted of two layers of 0.25 mm thick ceramic insulation cloth. The strip heaters were placed in between the two layers. The half-coil along with the ground insulation was cured at 150 $^{o}$C for 30 min. Fig. 8 shows the two half coils with the ground insulation ready to be assembled into the reaction fixture. Fig. 9 shows the schematic of the heater assembly in HFDA-02.

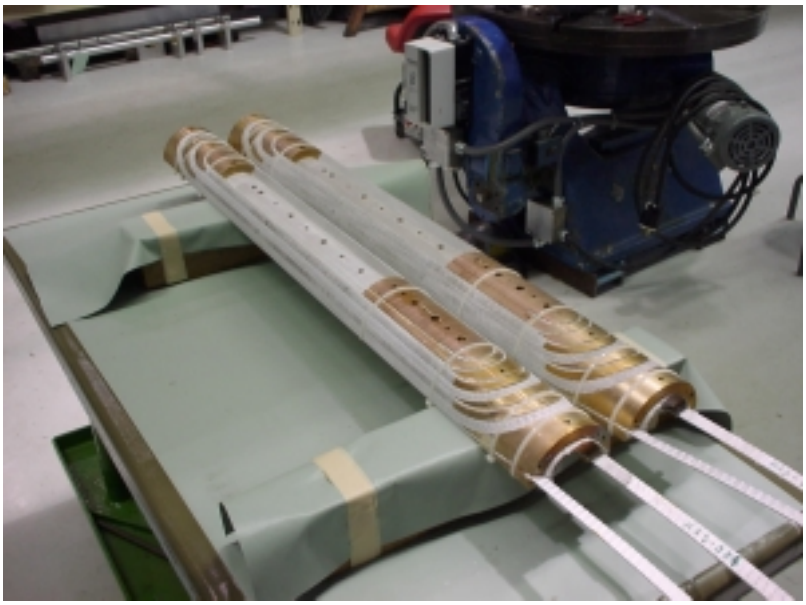

**Fig. 7**: *Two half-coils after winding and curing.*

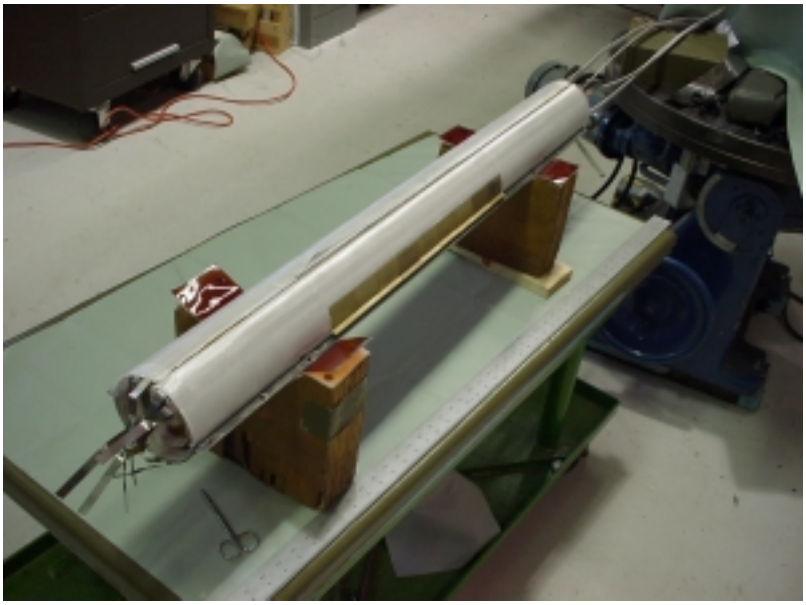

**Fig. 8**: *Two half-coils with ground insulation and strip-heaters.*

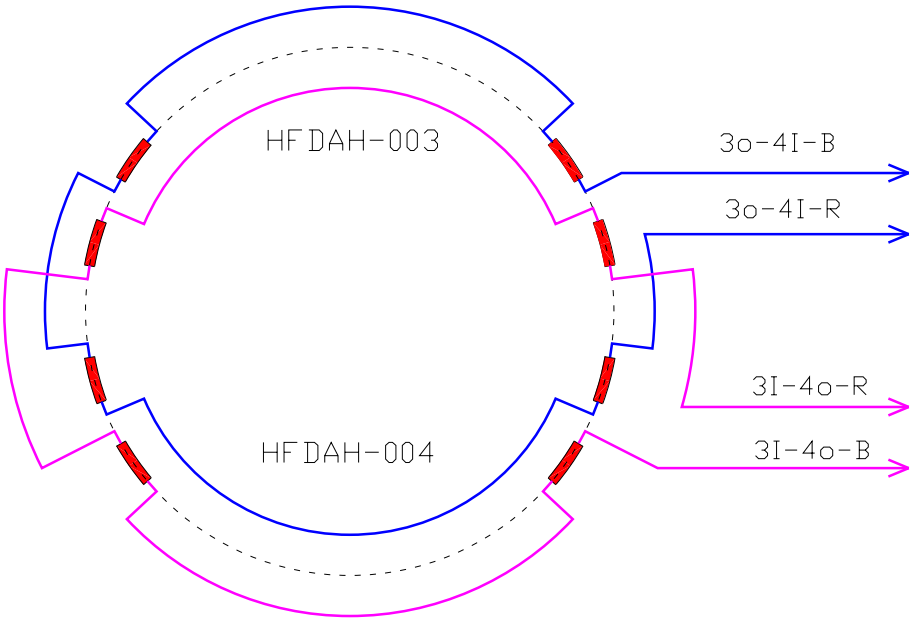


**Fig. 9**: *HFDA-02 heaters wiring diagram.*

## 3.4 Coil Electrical and Mechanical Measurements

Electrical measurements (L, Q and R) were also taken on both the half coils to check for possible turn-to-turn shorts. The data is shown in Table 2. Both the coils have similar values and match the theoretical estimates, which indicate that the coils are free from turn-to-turn shorts. Note that the inductance, L and Q were measured at 1 kHz. Resistance was measured using four-wire technique at 0.1 A.

| | **Resistance mΩ** | **Inductance μH** | **Q** |
|---|---|---|---|
| **HFDAH-03** | 60.07 | 243.94 | 6.94 |
| **HFDAH-04** | 59.52 | 244.34 | 6.99 |

**Table 2**: *Electrical measurements on the cured half-coils.*

The azimuthal size in the straight section of the two half-coils was measured at two positions at varying pressures. Fig. 10 shows the data with respect to the nominal size. Note that these measurements were taken before the installation of the ground insulation. The mean azimuthal size of HFDAH-03 is 1.6 mm below the nominal size, where as HFDAH-04 is 1.4 mm below the nominal size. The average increase in size due to reaction for a cable with insulation is about 100 μm. For a total of 13 turns, the increase will be 1.3 mm, but HFDAH-03 is 1.6 mm below the nominal size. So 250 μm thick ceramic insulation layer was added at the parting plane to compensate for the size.

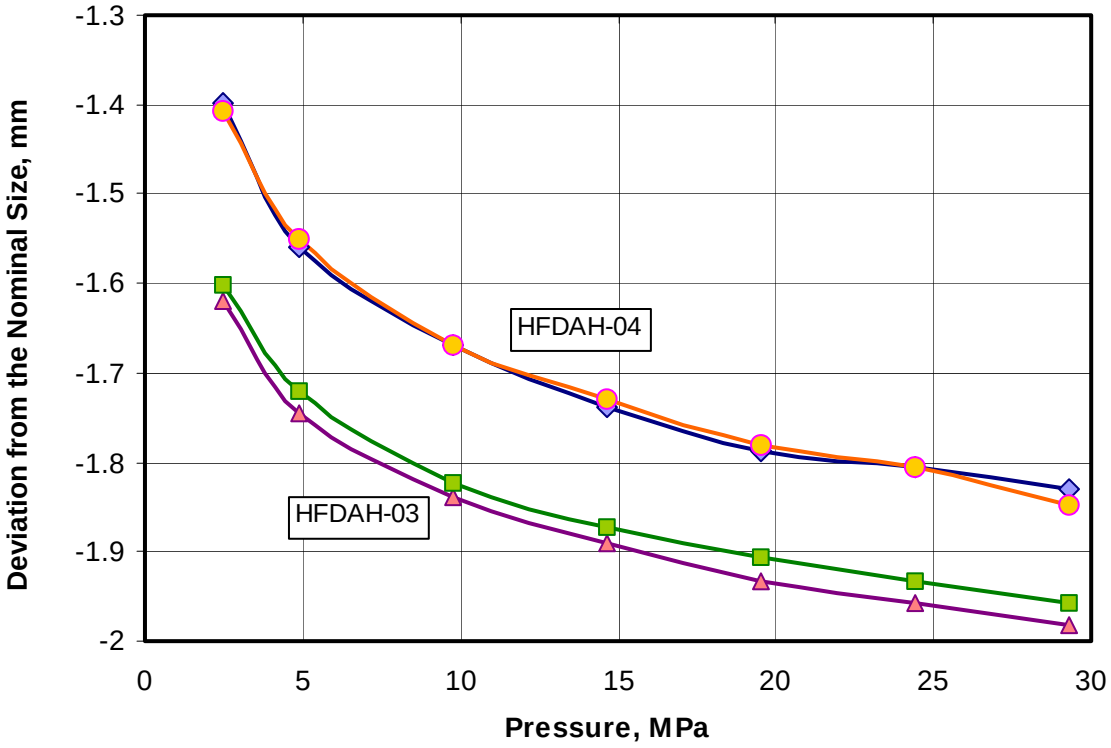


**Fig. 10**: *Azimuthal coil size variation with pressure at two positions along the straight section of the coil.*

## 4.0 COIL REACTION

As stated earlier several precautions were taken to avoid tin leakage, which was observed in HFDA-01 coils. First we reduced the overall azimuthal size of the coils to allow for the expansion during reaction. Second, the reaction cycle was modified to have a low temperature step in the beginning to allow tin to diffuse in solid phase. The reaction cycle followed for HFDA-02 is given in Table 3. Sample cables with artificial defects such as scratches and matrix poking were heat-treated with the proposed reaction cycle both at Fermilab and KEK and found no tin leakage.

| | Ramp Rate $^{o}$C/hr | Temperature $^{o}$C | Dwell Time hr |
|---|---|---|---|
| **Step - 1** | 25 | 210 | 100 |
| **Step - 2** | 50 | 340 | 48 |
| **Step - 3** | 75 | 650 | 180 |

**Table 3**: *Heat-treatment cycle for HFDA-02.*

The two half-coils were assembled into the reaction fixture and then placed inside the retort. Since the coils were undersized, the two halves of the reaction fixture closed very easily. Thermocouples were attached to the either end of the stainless steel mandrel to measure the temperature of coil and a third

one was placed inside the retort to measure the temperature of the argon. Fig. 11 and Fig. 12 shows the measured temperature profile during ramp up from room temperature to 210 $^{o}$C and from 210 $^{o}$C to 340 $^{o}$C respectively. Note that for the Step-3 the ramp-up has similar temperature profile except that by the time the temperature of the furnace reaches 500$^{o}$C the coil temperature catches up with the furnace and there after the temperature of the furnace and the coil remain the same. Fig. 13 shows the measured temperature profile of the coil during cooling down. A major fraction in the difference between the measured critical current density between the samples from the tube-furnace and the big-furnace could be attributed to their differences in the ramp-up and cool-down temperature profiles. Note that in the tube furnace the coil temperature ramps-ups and also cools-down more rapidly than in the big-furnace. Separate experiments will be conducted to understand this effect and to optimize the heat-treatment cycle for the big-furnace.

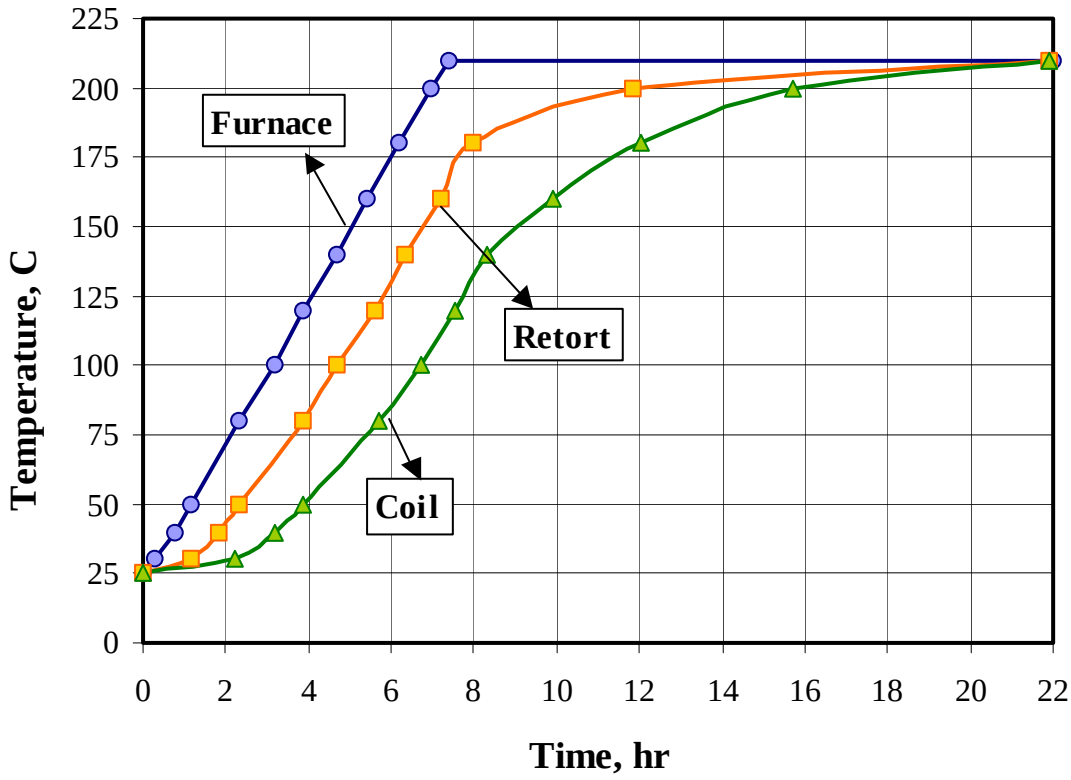


**Fig. 11:** *Measured temperature profile of the coil, retort and the furnace during ramp-up from room temperature to 210 $^{o}$C.*

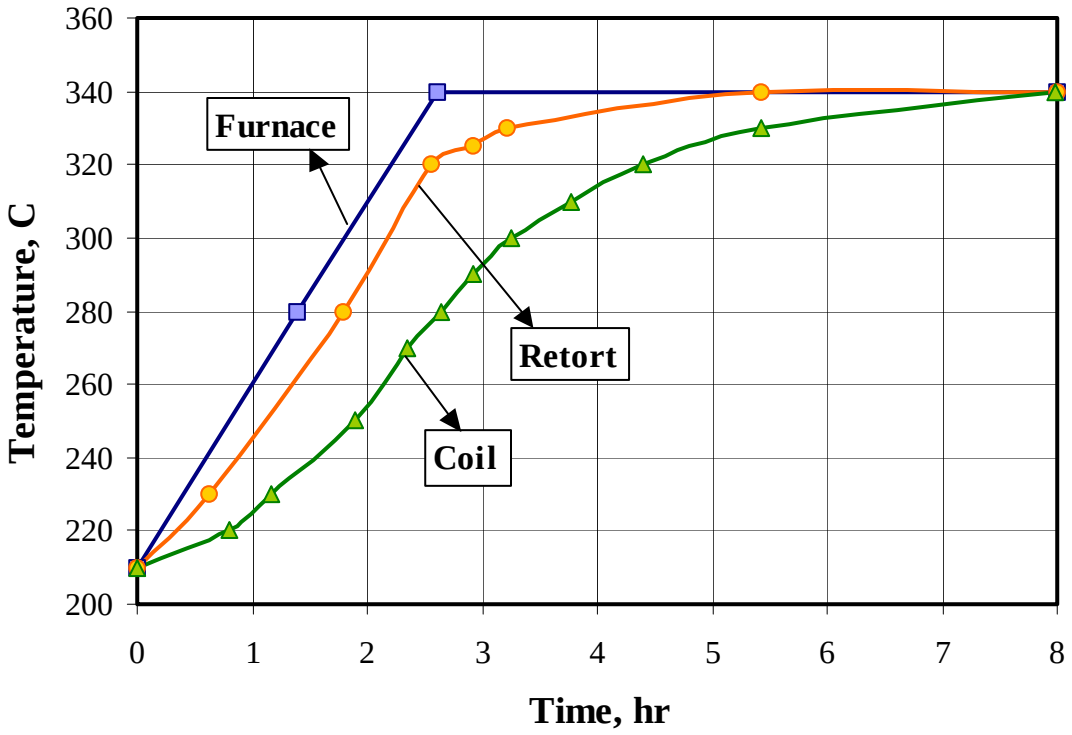


**Fig. 11:** *Measured temperature profile of the coil, retort and the furnace during ramp-up from 210 °C to 340 °C.*

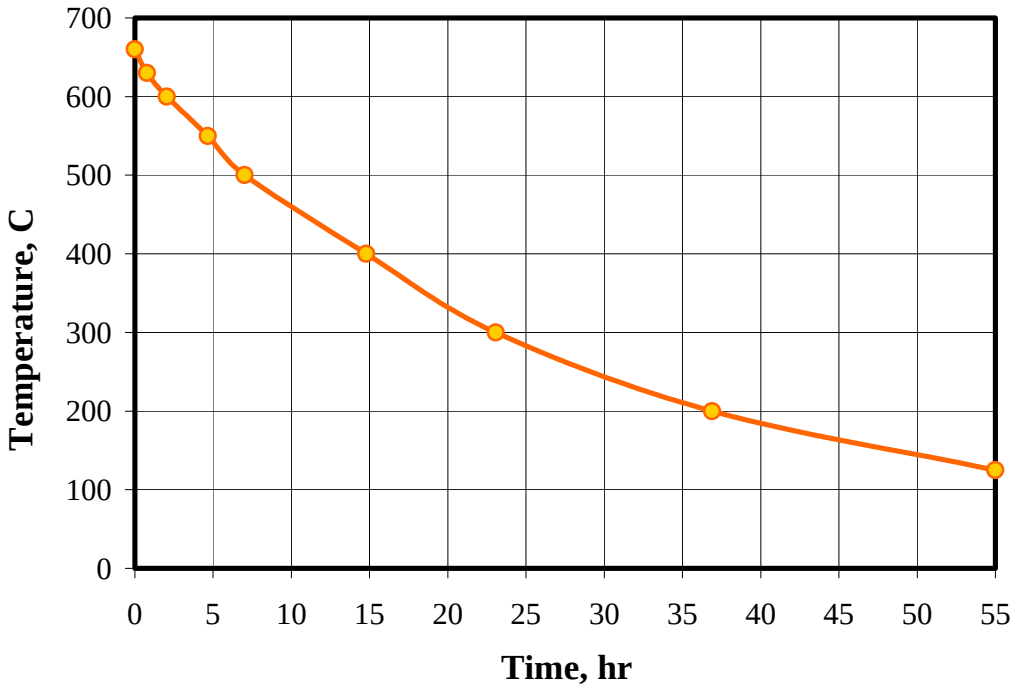


**Fig. 13**: *Measured temperature profile of the coil during cooling down.*

## 5.0 SPLICE JOINTS

The first step after the coil reaction was to perform the $Nb_3Sn$ to NbTi splice joints. Each splice joint (total 4) consists of one $Nb_3Sn$ cable between two NbTi cables enclosed in a copper cage. The procedure followed was similar to that of in HFDA-01. During the splicing operation, HFDAO-003 lead was broken. It was later repaired by splicing near the end-saddle of that coil. The end-saddle was removed and modified to create enough space for the splice joint. Fig. 14 (a) shows the repaired splice joint. Fig. 14 (b) shows the rest of the four splice joints. After this operation it was decided to change the splicing procedure and a new tooling was to be designed for future coils.

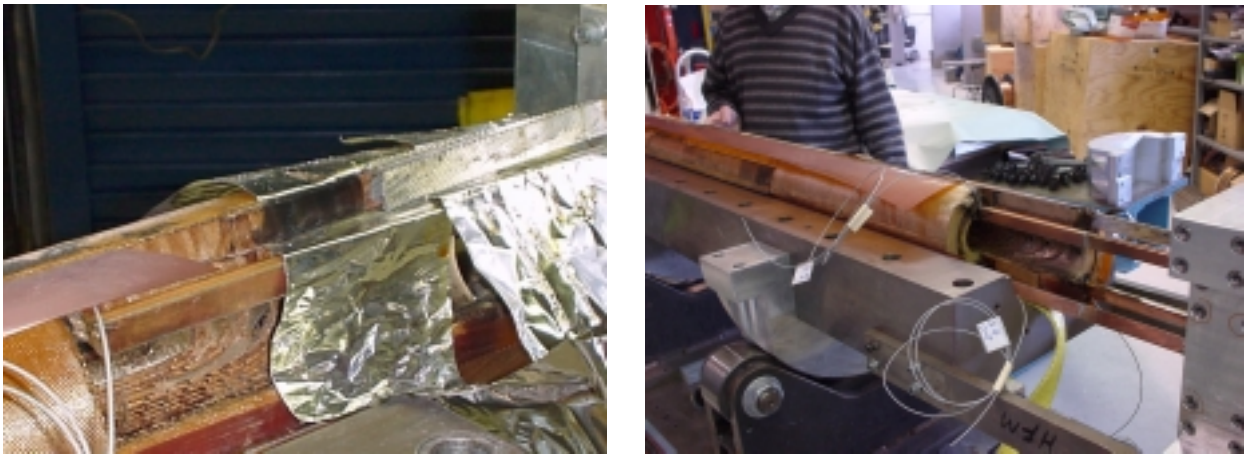

**Fig. 14**: (a) *HFDAO-003 splice joint*. *(b) Other three splice joints.*

## 6.0 EPOXY IMPREGNATION

The reacted coil was transferred from the reaction fixture to the impregnation fixture using rollover assembly. The coil was inspected during this transfer and no tin-leakage was observed. The length of the half-coil after reaction grew by about 2 mm unlike in HFDA-01, where the coils grew by about 9 mm.

The two halves of the impregnation fixture were closed without applying any additional pressure. Fig. 15 (a) shows the fixture with all the plumbing and the support fixture used to hold it at an angle inside the vacuum chamber. The impregnation procedure followed was similar to that of HFDA-01. However a few modifications were done to improve the vacuum level. The on/off value, which was on the epoxy-mixing vessel, was removed to eliminate any air leakage. A better and sturdy flow meter was also built to control the flow rate. The impregnation went smoothly and took about 5 hr. to complete. The weight of the coil assembly along with the impregnation fixture was measured before and after impregnation to compute the volume of epoxy in the coil assembly. A total of about 8 lbs [3.5 kg] of epoxy was consumed. Since the density of CTD-101K is 0.11 lbs/$in^3$ [3 g/$cm^3$], the equivalent volume of epoxy is 72 $in^3$ [1167 $cm^3$] or approximatly1.2 liters. Fig. 15 (b) shows the impregnated coil assembly.

**(a)** **(b)**

**Fig. 15**: *(a) Impregnation fixture fixed on top of the support fixture with all the necessary plumbing. (b) Epoxy impregnated coil assembly.*

Electrical measurements (L, Q, and R) were performed on the impregnated coil assembly. Table 4 shows the data. For comparison measurements taken before reaction were also included in the table. The resistance of the coil assembly after reaction increased by about 70%. The Q decreased by the same amount as the inductance of the coil remained constant before and after reaction. Most importantly the two coils have similar values, which indicate that there are no turn-to-turn shorts. Note that L and Q are measured at 1 kHz.

Hi-Pot tests up to 1 kV were also performed on the impregnated coil assembly to check leakage between coil to ground, coil to heaters and heaters to ground. The current leakage was less than 0.04 μA at 1 kV. Note that the acceptable leakage is about 0.5 μA at 1 kV.

| **Parameter** | **Before Reaction** | | **After Reaction and Impregnation** | |
|---|---|---|---|---|
| | **HFDAH-03** | **HFDAH-04** | **HFDAH-03** | **HFDAH-04** |
| **Resistance, mΩ** | 60.07 | 59.52 | 101.58 | 102.23 |
| **Inductance, μH** | 243.94 | 244.34 | 213.45 | 214.61 |
| **Quality Factor** | 6.99 | 6.94 | 3.63 | 3.64 |

**Table 4**: *Electrical measurements of coil after reaction and impregnation.*

## 7.0 INSTRUMENTATION

One outer pole piece on each half-coil was mold released before epoxy impregnation so that we can remove them after impregnation (Fig. 15(b) shows the coil with one pole piece removed). Two outer pole pieces were modified to accept capacitance gauges and were placed at these locations. Resistive gauges were mounted on the circumferential grooves made on the aluminum spacers. Fig 16 shows the layout of gauges in the magnet cross-section. The capacitance gauges measure the azimuthal stress in the

outer layer of the half-coils while the resistive gauges measure the azimuthal stress in the aluminum spacers.

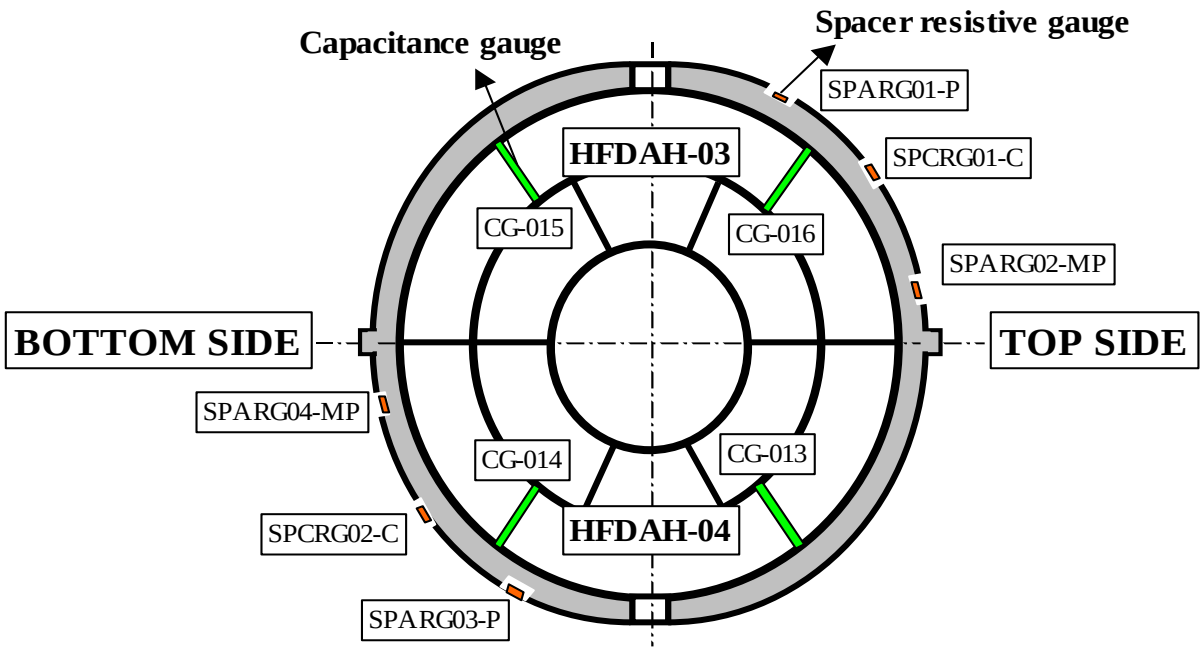


**Fig. 16**: *Layout of gauges in the magnet cross-section.*

## 8.0 YOKING

Aluminum spacers were first installed around the two half coils. The instrumented coil assembly with the spacers was placed into the lower yoke packs that were already stacked in the bottom half of the contact tooling. The upper half of the yoke packs was then installed on top of the coil/spacer assembly. Finally the contact tooling was placed on top of the yoked assembly.

The pump pressure was increased in 1000 Psi increments and the gauge readings were recorded. During the first loading we noticed a large asymmetry in loading between topside and bottom side of the coil assembly (see Fig. 16). Note that top and bottom side represents half of each coil. The asymmetry in stress was computed to be equivalent to 2 mils of radial size difference between the two sides. A total of 3 mil Kapton shim was added in the radial direction to the bottom side and a 1 mil radial shim was added to the topside of the coil and was reassembled in the yoke halves. Fig. 17 shows the evolution of azimuthal stress in the coil with the pump pressure. The dashed line represents ANSYS predictions. There is still a difference of 30 MPa between the two sides of the coil. HFDA-01 was measured using CORDAX machine and we observed a 2 mil shift in the outer pole pieces with respect to the center of the coil assembly. Hence the spacers on one side will have more interference with the outer pole pieces than on the other side, which will then result in the asymmetry in the coil stresses. Note that these measurements were taken after HFDA-02 assembly. Fig. 18 shows the evolution of azimuthal stress in the spacer. The dashed lines again represent the ANSYS predictions. Even though the mid-plane stress matches with the ANSYS data, the stress at the pole is about 50 MPa more than the computed values.

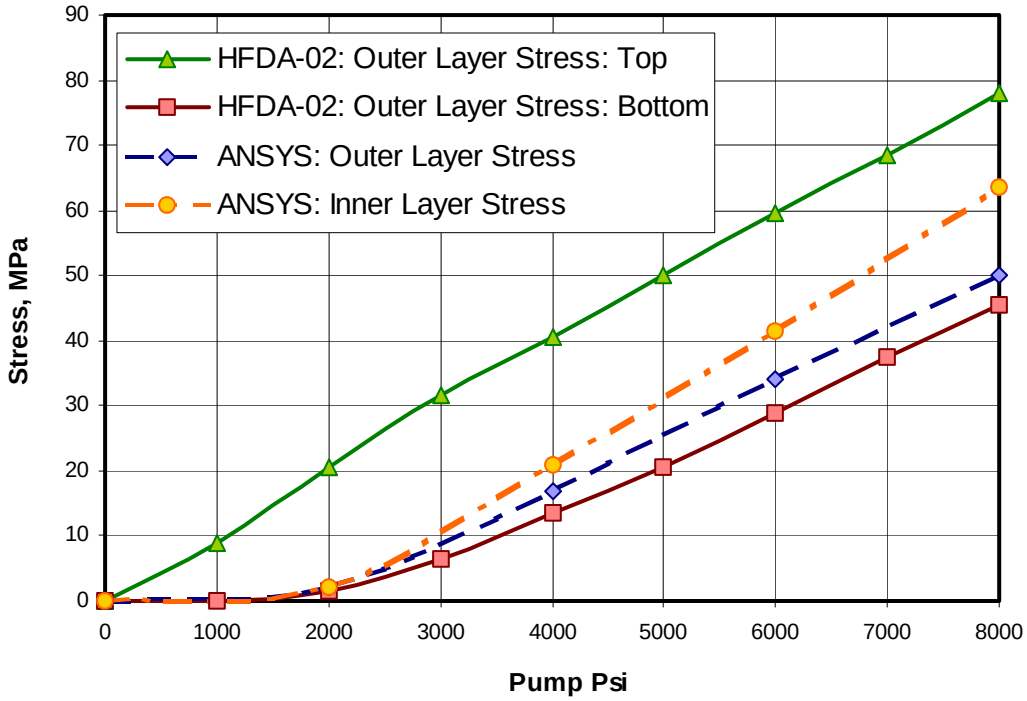


**Fig. 17**: *Evolution of azimuthal stress in the outer layer of coil with pump pressure.*

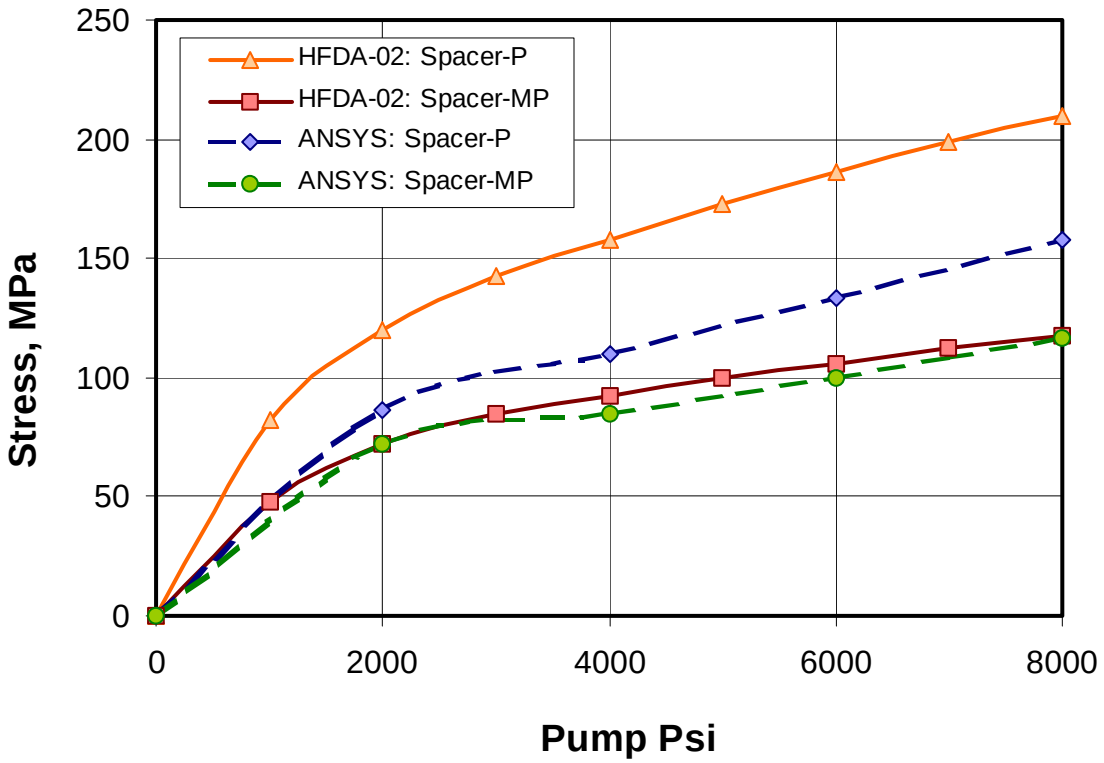


**Fig. 18**: *Evolution of the azimuthal stress in the spacer. Note that 'P' represent pole and 'MP' represent mid-plane. Each experimental data represent average between two gauge readings, one on topside spacer and the other on bottom side spacer.*

At 8000 pump Psi, the gap between the yoke halves was close to the nominal value and the clamps were inserted using a separate set of pusher blocks. Fig. 19 (a) shows the set-up during yoking/clamping operation. Two clamps, one on each side were inserted simultaneously starting from the middle of the magnet. Note that during the entire operation the coil resistance was monitored to make sure we do not have any turn-to-turn shorts. Fig. 19(b) shows the yoked magnet. Table 5 gives the summary of the data collected during yoking. The ANSYS data is also given in the table. The azimuthal stress in the coil outer layer pole region after springback is about 30 MPa in the topside and 8 MPa in the bottom side.

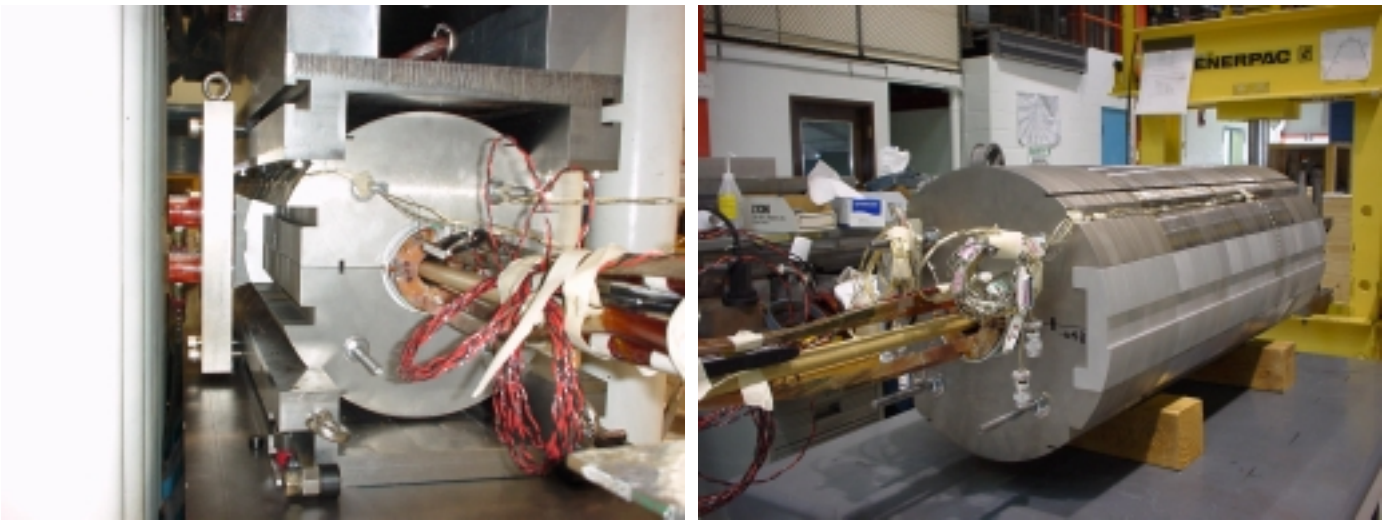


**(a)** **(b)**

**Fig. 19**: *(a) Magnet assembly in the yoking press. (b) Yoked magnet.*

| | UNDER PRESS MPa | DURING CLAMPING MPa | AFTER SPRING BACK MPa | AFTER WELDING SKIN MPa |
|---|---|---|---|---|
| **HFDA-02** | | | | |
| **OUTER LAYER TOP SIDE** | 85 | 94 | 30 | 55 |
| **OUTER LAYER BOTTOM SIDE** | 45 | 60 | 8 | 29 |
| **SPACER-POLE** | 213 | 223 | 115 | 159 |
| **SPACER-MIDPLANE** | 119 | 126 | 95 | 104 |
| **CLAMP** | | | 40 | 42 |
| **SKIN** | | | | 180 |
| **ANSYS** | | | | |
| **OUTER LAYER POLE** | 50 | | 20 | 60 |
| **SPACER-POLE** | 160 | | 108 | 165 |
| **SPACER-MIDPLANE** | 118 | | 84 | 117 |
| **CLAMP** | | | 67 | 45 |
| **SKIN** | | | | 216 |

**Table 5**: *Summary of data collected during yoking and skinning.*

## 9.0 SKINNING AND END-PLATE INSTALLATION

The next step in the magnet assembly is to weld the two skin halves on to the yoked assembly. First the skin alignment keys were inserted into the grooves provided in the aluminum clamps. The whole assembly is then gently placed in the lower half of the skin that is already installed in the welding press. The upper half of the skin is then installed on the magnet. The two skin halves were compressed at 600 pump Psi during welding operation. After each weld pass, the distance between the top and bottom pushers was measured to compute weld shrinkage. Simultaneously the gauge readings were recorded to monitor the increase in coil stress with weld shrinkage. Fig. 20 shows the evolution of stress in the coil with the weld shrinkage. At the nominal weld shrinkage of about 0.4 mm, the stress in the coil according to the ANSYS calculations should be around 60 MPa. Even though the topside of the coil assembly was very close to the nominal value after the first filler pass, the stress in the bottom side of the coil assembly was only 22 MPa. Three more filler passes were added to increase the stress in the bottom side of the coil to 30 MPa. Table 5 summarizes the data after welding along with the ANSYS data. The stress in the skin was also monitored during welding operation. The mean azimuthal stress in the skin is about 180 MPa.

After welding the ends of the skins were cut to the right dimensions. The end plates were then welded on both lead and return ends to provide axial support to the coils. Finally the twist along the length of the magnet was measured using twist-measuring device. Fig. 21 shows the variation of the twist along the length of the magnet.

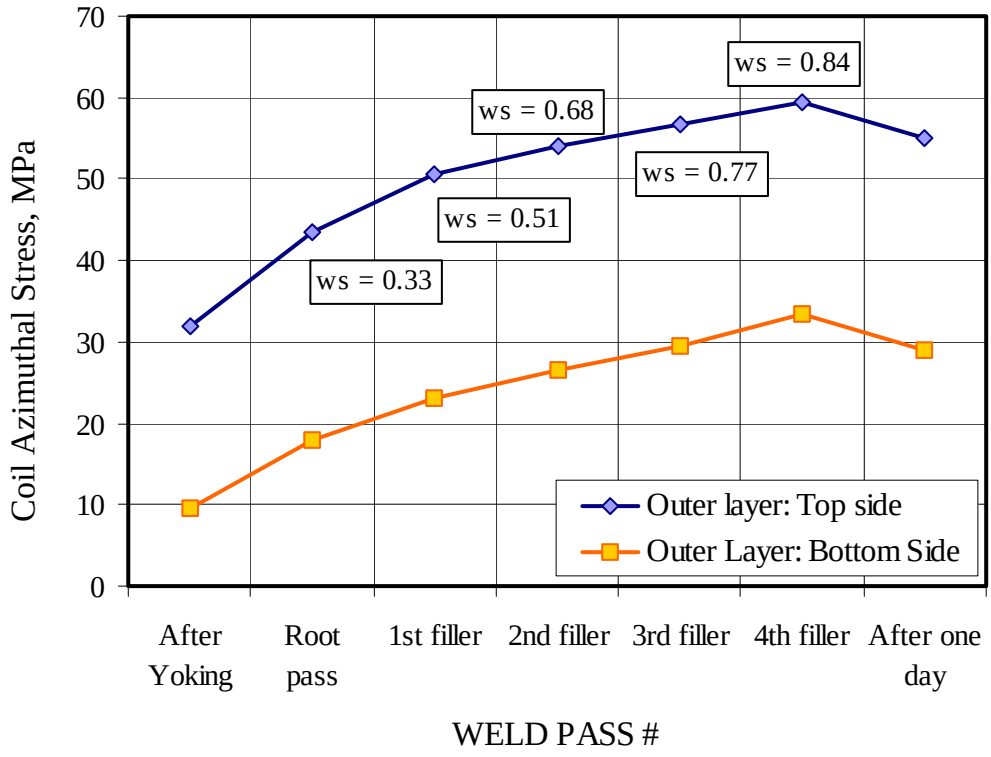


**Fig. 20**: *Evolution of coil stress with weld shrinkage.*

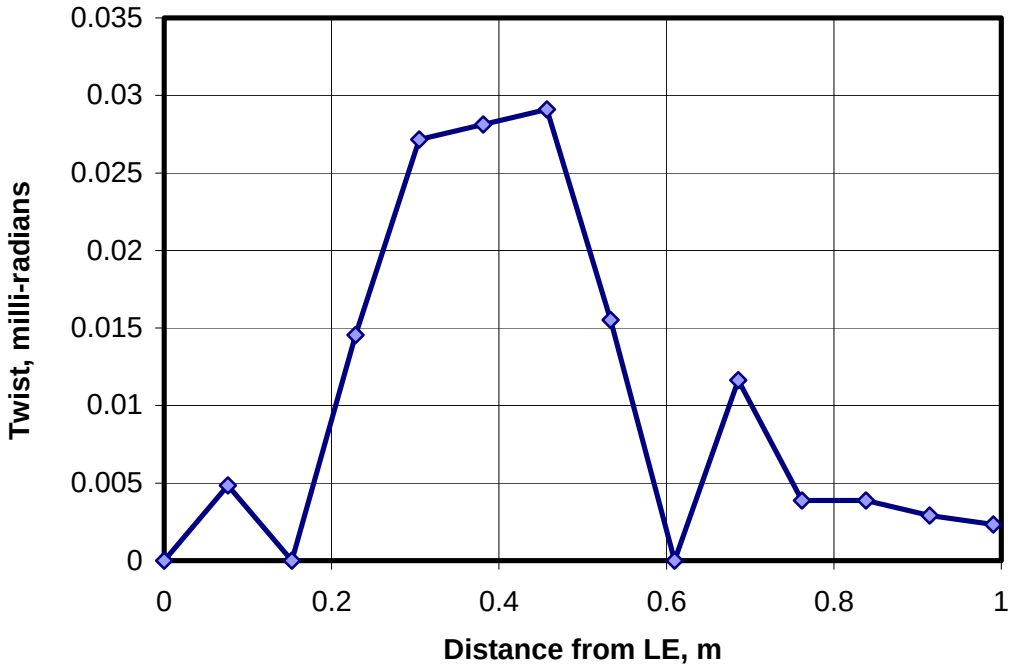


**Fig. 21**: *Variation of twist along the length of the magnet*.

## 10.0 FINAL ASSEMBLY

Once the end plates were welded, the bullets were installed on both LE and RE. Four bullets per end were torqued until each bullet sees 500 lbs of force. Note that the bullets were installed with strain gauges and were calibrated both warm and cold.

Five gauges were installed along the length of the skin to measure the longitudinal stress in the skin during excitation. The last mechanical assembly involved performing the half-coil splices. The outer layer leads from both the half-coils were spliced together and captured in a G-10 box. The inner layer leads were used as power leads for the magnet.

Several voltage taps were installed on the lead cables before installing the splice box assembly as per drawing MB-376907. All the wires were finally terminated into hypertronic connectors to be hooked up in VMTF.

Electrical measurements were made be on the magnet just before shipping it to the VMTF. Table 5 summarizes these measurements. L and Q were measured at different frequencies and Fig. 22 shows the variation of the magnet inductance with frequency. Note that the theoretical estimate is at zero frequency. However the instrument could go only down to 20 Hz.

Hi-pot tests were also performed on the magnet and the current leakage between coil to ground, heater to ground and coil to heater was less than 0.04 μA at 1.0 kV.

| | Resistance mΩ | Inductance, mH | | Quality Factor | |
|---|---|---|---|---|---|
| | | At 1 kHz | At 20 Hz | At 1 kHz | At 20 Hz |
| **HFDAH-03** | 98.60 | 0.115 | 0.351 | 1.22 | 0.20 |
| **HFDAH-04** | 99.26 | 0.118 | 0.357 | 1.22 | 0.20 |
| **Total Magnet** | 197.95 | 0.306 | 1.091 | 1.38 | 0.57 |

**Table 5**: *Electrical measurements on the half-coils and the total magnet.*

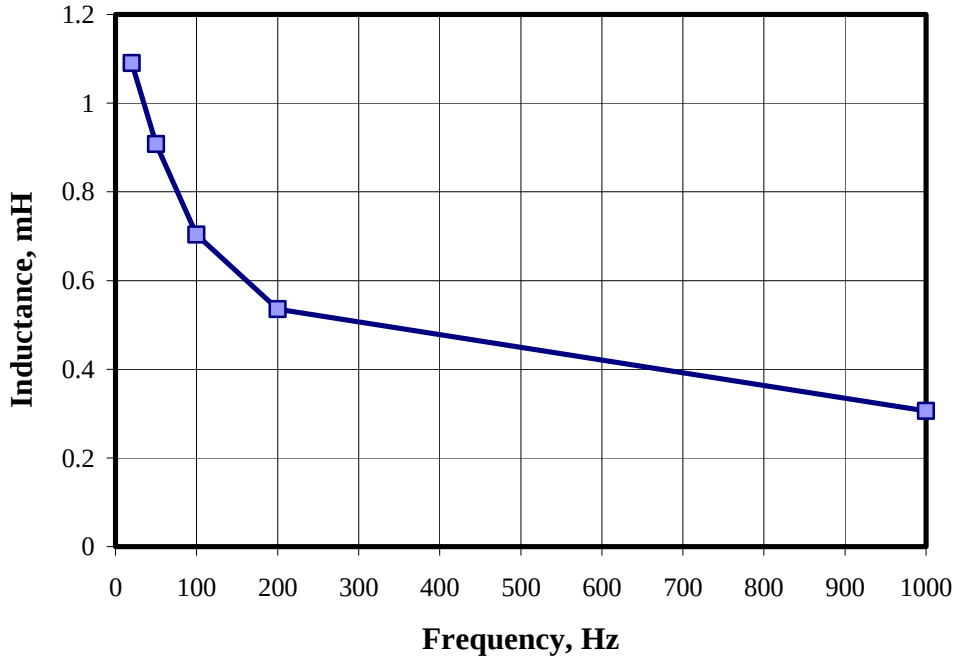


**Fig. 22**: *Variation of the magnet inductance with frequency.*

Fig. 23 shows the schematic of the longitudinal section of the magnet. The dimensions shown in the figure are the nominal dimensions.

## 11.0 SUMMARY

The second shell-type $Nb_3Sn$ high field dipole magnet took about 5 months to complete. It was delivered to VMTF for testing on May 03, 2001.

Several issues such as coil size, tin-leakage observed in HFDA-01 have been addressed in this magnet. However the asymmetry in the coil prestress between the topside and the bottom side of the coil assembly needs to be looked into. We now know that there is a shift in outer pole pieces with respect to the center of the coil assembly. This comes from the asymmetry in the impregnation tooling. Extreme care should be taken to properly shim the impregnation tooling for the next magnet.

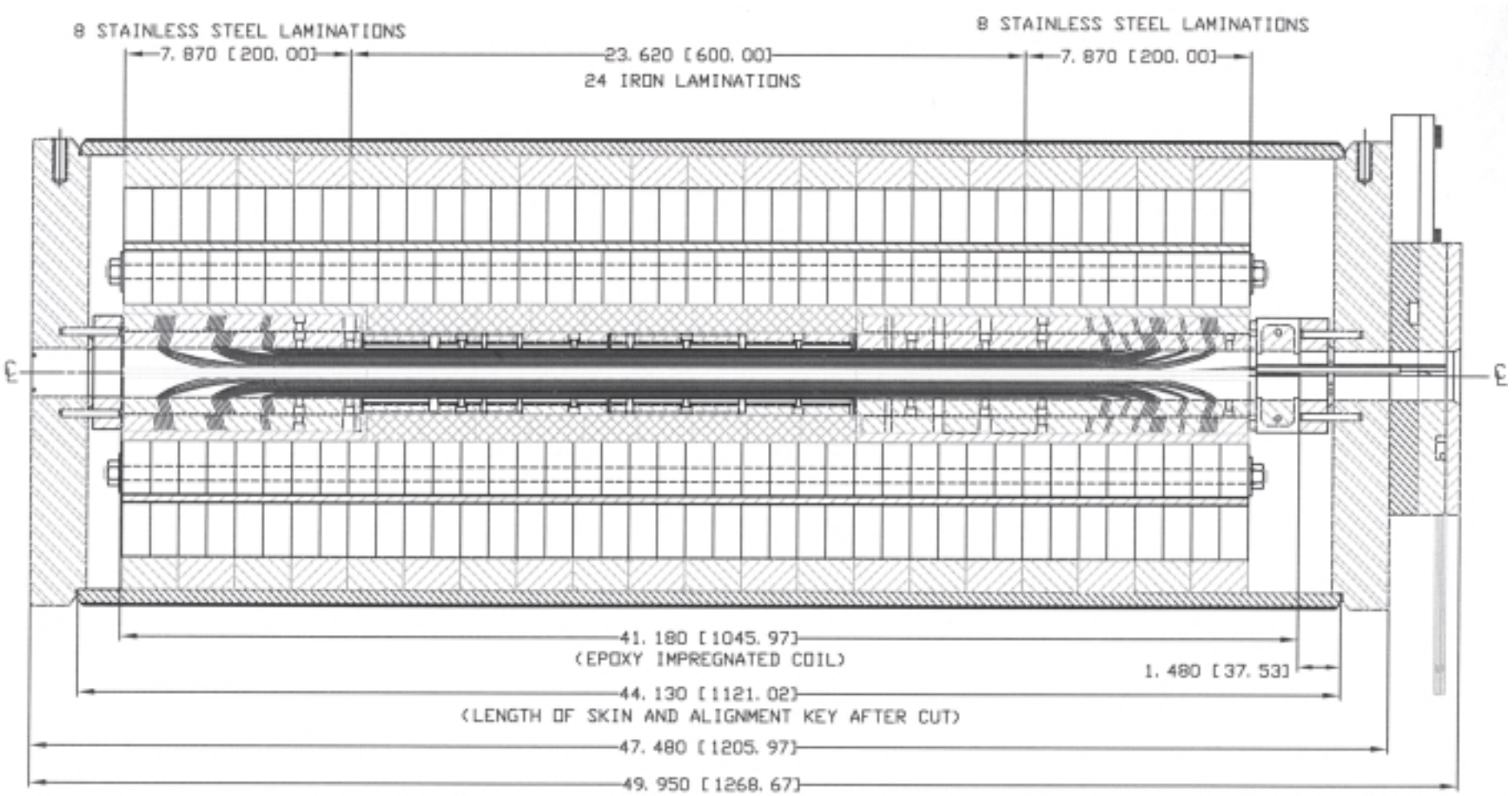


**Fig. 23**: *Longitudinal section of the magnet. Note that the dimensions in the brackets are in mm*